RSC Advances

ROYAL SOCIETY OF CHEMISTRY

www.rsc.org/advances

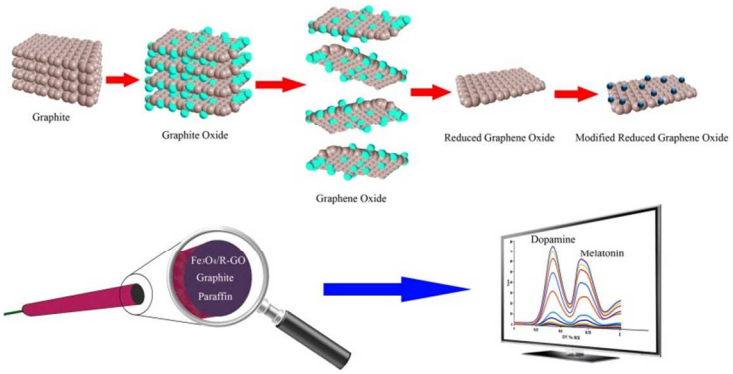

Electrochemical sensor based on a new nanocomposite of graphene/Fe_3O_4 has been fabricated for simultaneous determination of melatonin and dopamine.

RSC *Advances* RSCPublishing

ARTICLE

Simultaneous and sensitive determination of melatonin and dopamine with Fe_3O_4 nanoparticles-decorated reduced graphene oxide modified electrode

Cite this: DOI: 10.1039/xoxxoooooox

Received ooth January 2012,
Accepted ooth January 2012

DOI: 10.1039/xoxxoooooox

www.rsc.org/

H. Bagheri, [a,*] A. Afkhami, [b] P. Hashemi, [b] and M. Ghanei [a]

An electrochemical sensor was developed for melatonin and dopamine detection using graphene (Gr) decorated with Fe_3O_4 magnetic nanoparticles on a carbon paste electrode (CPE). The structure of the synthesized nanocomposites and the electrodes composition were confirmed by X-ray diffraction (XRD) spectrometry, Fourier transform infrared (FT-IR) spectrometry, thermogravimetric analysis (TGA) and scanning electron microscopy (SEM). Electrochemical studies revealed that modification of the electrode surface with Gr/Fe_3O_4 nanocomposite significantly increases the oxidation peak currents but reduces the peak potentials of melatonin and dopamine. The peak currents in square wave voltammetry of melatonin and dopamine increased linearly with their concentration in the range of 0.02-5.80 μM. The limits of detection ($3s_b/m$) were found to be 8.40×10^{-3} and 6.50×10^{-3} μM for melatonin and dopamine, respectively. Also the effect of some interfering compounds such as glucose, ascorbic acid, pyridoxine, serotonin, uric acid and others on the determination of melatonin and dopamine was studied, and all have no significant effect on the assay recovery. Moreover, its practical applicability was reliable and desirable in biological fluids and pharmaceutical samples analysis.

Introduction

Melatonin (ML) and dopamine (DA) have been of interest to neuroscientists and chemists.[1,2] Both ML and DA are abundant neuromodulators located in vertebrate retina. In vertebrates, the functions of ML are numerous. For example, it influences circadian rhythms, acts as a neuromodulator and as sleep regulator, inhibits DA release in the hypothalamus and retina. Also, ML is involved in the aging process, pubertal development in some species and modulates blood pressure. Furthermore, ML is a critical free radical scavenger and upregulates the immune response.[1,2] DA is a neurotransmitter that is widely distributed in the mammalian central nervous system for message transfer, and it plays an important role in the function of the central nervous, renal and hormonal systems. The DA deficiency and variations in ML levels have been linked to Parkinson's disease.[1-3] Also, abnormal metabolism of neurotransmitters, particularly DA and ML, is frequently observed in individuals with phenylketonuria and is believed to be involved in related psychological and psychiatric symptoms.[3]

The accurate detection of DA and ML in biological fluids such as blood and urine due to consider their low concentrations and generally complex biological matrix is not an easy task.[4-6] Because of their important roles in numerous pathological, physiological and biological processes, the improper levels of these compounds in the body can lead to various diseases. Therefore, the development of a sensitive and selective method for their simultaneous determination is highly desirable for analytical applications and in researches in the field of physiological functions and diagnostic. The common instrumental techniques like high performance liquid chromatography (HPLC), radioimmunoassay (RIA) and Enzyme-linked immunosorbent assay (ELISA) enable determination of DA and ML.[5-8] In spite of all the advantages, high cost, low sensitivity and complication in these methods and usually single compound determination capability with immunological assay are considered as serious drawbacks.

Since the DA and ML are electroactive compounds, they can be detected by electrochemical methods based on oxidation processes.[9,10] However, one of the biggest challenges of electrochemical detection of DA and ML in biological matrixes is the coexistence of many interfering compounds. For example, ascorbic acid (AA) usually coexists with DA in extracellular fluid at a high concentration level, nearly 100 to 1000 times higher than DA. Moreover, DA and AA can be oxidized at practically the same potential at bare electrodes, resulting in the peak overlapping as well as poor response resolution in DA determination.[11] Also, because tryptophan has a similar electroactive group as ML, its oxidation potential is close to that of ML and thus affect its oxidation peak current.[12] To solve these problems, the use of chemically modified electrodes (CMEs) instead of bare ones is preferred.

The electrochemical performance of a CME is strongly affected by the electrode materials.[13-15] Chemically modified matrices should possess a high conductivity and a preferably low electron transfer resistance on their selective surface. Furthermore, it is also beneficial if there is a large surface area for interacting of target species. For these reasons, there is an emerging interest in nanostructured surfaces to be used in voltammetric determination.[13-15] A considerable number of research reports emerged recently, underlining the importance of utilizing Gr for electrochemical sensors and proving the suitability of the material for the detection of biomolecules.[16-18]

Gr is a two dimensional sheet of carbon atoms bonded by sp^2 bonds. This configuration provides the material with extraordinary properties, such as large surface area, theoretically 2630 m^2/g for a single layer.[19,20] It also shows excellent thermal ($k=5\times10^3$ W m^{-1} K^{-1}) and electrical conductivity (r = 64 mS cm^{-1}). Gr is considered a zero-gap semiconductor, because it presents no gap between conduction and valance bands, so it might be considered a semiconductor or a metal. In physical properties, Gr has optical transparence, high mechanical strength (Young's modulus, 1100 GPa).[19] and high elasticity. The effective surface area of Gr materials depends highly on the layers, that is, single or few layers with agglomeration should be expected to exhibit a higher effective surface area. Therefore, numerous metal oxides and polymers have been added into Gr to enlarge the specific surface area of the pristine Gr. [21] Therefore, physico-chemical properties of the Gr can be tailored by chemical modification of its surface.

New hybrid materials based on Gr and nanoparticles have also been developed quickly in the last decade not only because they display the individual properties of Gr and the nanoparticles, but also because they can exhibit additional synergistic properties. These nano-sized materials offer many advantages due to their size and unique physic-chemical properties.[22,23] Several types of magnetic Gr have been synthesized by decorating Gr with different magnetic nanoparticles in order to provide additional advantages.[24-27] Magnetite (Fe_3O_4) is one of the most commonly used magnetic nanomaterials because of its biocompatibility, catalytic activity, high saturation magnetization, low toxicity and easy preparation.[28] Some reports can be found concerning the application of Fe_3O_4 in sensing applications.[26,27] Consequently, Gr-Fe_3O_4 composite combines the respective advantages, such as huge surface area, good electronic conductivity and excellent catalysis, which can be used to detect hydrogen peroxide, guanosine, N-acetylcysteine and etc.[29-31]

In the present work, we describe the findings of our continuing investigations of the properties of modified Gr composites.[18,24,25] The objective of this work is to introduce an effective composite to design a sensitive and selective interface for simultaneously electrochemical determination of ML and DA in the presence of possible interferences by square wave voltammetry (SWV). Gr-Fe_3O_4 nanocomposite modified CPE displays good sensitive oxidation towards ML and DA with well separated oxidation peaks for each species. This could be ascribed to the synergistic effect of both Gr and Fe_3O_4 nanoparticles. Modified Gr with Fe_3O_4 nanoparticles leads to enhance in signal responses. This is due to mutual interactions. A comparison with a sensor based on the use of CPE and the individual components revealed that such properties can be ascribed to the ensemble behavior of the nanostructured materials. It was concluded that both of surface and the structure of Gr greatly improved with the deposited Fe_3O_4 nanoparticles, prompting the interfacial electron-transfer process for analytes species. The proposed sensor showed high sensitivity, selectivity with acceptable repeatability, reproducibility and good biocompatibility.

Experimental

The details of some experimental sections are given in Supporting Information (SI).

Preparation of reduced Gr-Fe_3O_4 composite

Gr oxide was prepared from natural graphite based on Hummers' method.[32] Gr-Fe_3O_4 composites were prepared via a hydrothermal method according to previous report.[33] Briefly, 0.036 g Gr oxide was first dispersed in 40 mL deionized water. At the same time, 0.270 g $FeCl_3.6H_2O$ and 0.528 g ascorbic acid were added into the beaker, forming a homogenous solution by ultrasonication. 10 mL hydrazine hydrate was added to the above solution under stirring. Then, the black solution was transferred into a 50 mL Teflon-lined stainless steel autoclave and heated at 180 ^{0}C for 8 h. After cooling to room temperature, solid precipitate was collected by centrifugation and washed three times with ultrapure water and alcohol, respectively. Finally, the Gr-Fe_3O_4 composites were obtained by drying at 60 ^{0}C under vacuum for 12 h.

Results and discussion

Characterization of Gr-Fe_3O_4/CPE

Fig. 1a shows the XRD patterns of the Gr oxide, Fe_3O_4 nanoparticles and Gr-Fe_3O_4 nanocomposite. The characteristic peak located at $2\theta=10^\circ$ was assigned to the (001) plane of Gr oxide. As shown in the pattern, the characteristic diffraction peaks at 28°, 34°, 42°, 52°, 54°, and 60° were indexed as the diffractions of the (2 2 0), (3 1 1), (4 0 0), (4 2 2), (5 1 1) and (4 4 0) crystalline planes of FCC Fe_3O_4 according to the standard XRD pattern of Fe_3O_4 (JCPDS, No. 79-0419).[33-35] The characteristic peak of Gr oxide at 10° disappeared for Gr-Fe_3O_4 pattern, confirming that Gr oxide was reduced to reduced Gr oxide with ascorbic acid and hydazine as the reducing agents. In addition, the broad peak at $2\theta=26^\circ$, corresponding to the stacked Gr sheets, was not observed, suggesting the decoration of Fe_3O_4 nanoparticles could efficiently reduce the aggregation of the Gr sheets. As can be seen, the pattern of Gr-Fe_3O_4 displayed obvious diffraction peaks of Fe_3O_4 nanoparticles, and the peak positions and relative intensities match well with the standard XRD data for magnetite, suggesting that prepared composite composed of pure crystalline Fe_3O_4 nanoparticles were successfully decorated onto the reduced Gr sheets.[33-35]

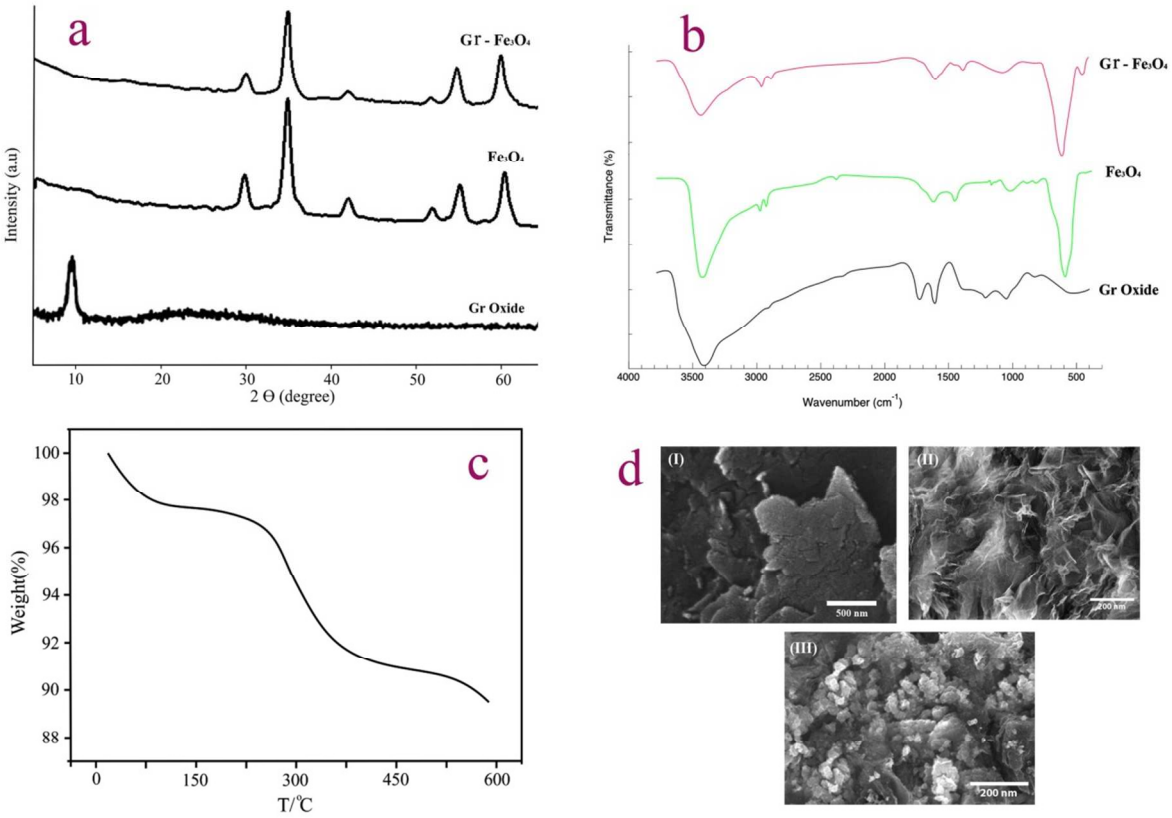

Fig. 1 XRD patterns of Gr oxide, Fe_3O_4 nanoparticles and Gr-Fe_3O_4 (a), FT-IR spectra for Gr oxide, Fe_3O_4 nanoparticles and Gr-Fe_3O_4 (b), TGA curve of Gr-Fe_3O_4 (c) and (d) SEM images from surface of CPE (I), Gr/CPE (II) and Gr-Fe_3O_4/CPE (III).

wavenumber of 625 cm^{-1}. This pattern corresponds to the Fe-O bonds, which is reported to belong to bulk magnetite.[28] FT-IR spectrum of Gr-Fe_3O_4 shows that the peaks at 625 and 560 cm^{-1} are denoted to stretching vibrations of Fe–O–Fe, clarifying the presence of iron oxide. Compared with Gr oxide, the intensity of absorption bands due to alkoxy, carboxy and carbonyl/ carboxy bonds disappeared or decrease. The results suggest that decoration of Gr with Fe_3O_4 has performed successfully.

The thermal property and composition of the Gr-Fe_3O_4 composite was characterized by TGA in an air atmosphere at a heating rate of 10 ˚C min^{-1}. As shown in Fig. 1c, for Gr-Fe_3O_4, the light mass loss (2.3 wt%) below 120 ˚C can be attributed to the evaporation of absorbed solvent. With increasing temperature, it showed a gradual mass loss spanning the range 250-500 ˚C, which can be ascribed to vaporization of various oxygen-containing functional groups, with a weight loss of 9.5%. When the temperature was increased to 550 ˚C, there were further weight losses for Gr-Fe_3O_4 composite due to the bulk pyrolysis of the carbon skeleton.[26,37]

The surface morphologies of different prepared electrodes were analyzed by SEM. Fig. 1d shows typical SEM images of the bare CPE, CPE modified with Gr and CPE modified with Gr-Fe_3O_4. Significant differences in the surface structure of electrodes are observed. The surface of the CPE was predominated by isolated and irregularly shaped graphite flakes and separated layers were seen. There was no conducting media available between carbon layers at the CPE, and charges could not be transferred along the vertical direction of planes because of the block of non-conductive binder. As shown in Fig. 1d, the Gr nanosheets are randomly packed on the CPE surface with folded or stacked structures. SEM image shows that the Gr sheets with lots of ripples are still observable, demonstrating the Gr structure remaining on the electrode surface. Rough irregularly shaped. As shown in Fig. 1d, the Gr-Fe_3O_4/CPE appears a surface which edges and wrinkles on the surface of Gr-CPE provide more electrochemical active sites, as compared to CPE surface with exhibits a wrinkled texture associating with the presence of flexible and ultrathin Gr sheets. It showed that Fe_3O_4 nanoparticles were well-distributed on Gr sheet. Furthermore, Gr absolutely prevents Fe_3O_4 nanoparticles from agglomeration and enables a good dispersion of these oxide particles over the surface. It is observed that the Fe_3O_4 nanoparticles are still strongly anchored on the surface of Gr sheets even after a long period of sonication, suggesting the strong interaction between Fe_3O_4 nanoparticles and Gr sheets. It is believed that the depositing and strong anchoring of Fe_3O_4 nanoparticles on the surface of Gr sheets enable fast electron transport through the underlying Gr layers to Fe_3O_4 nanoparticles to improve the electrochemical performance.[15]

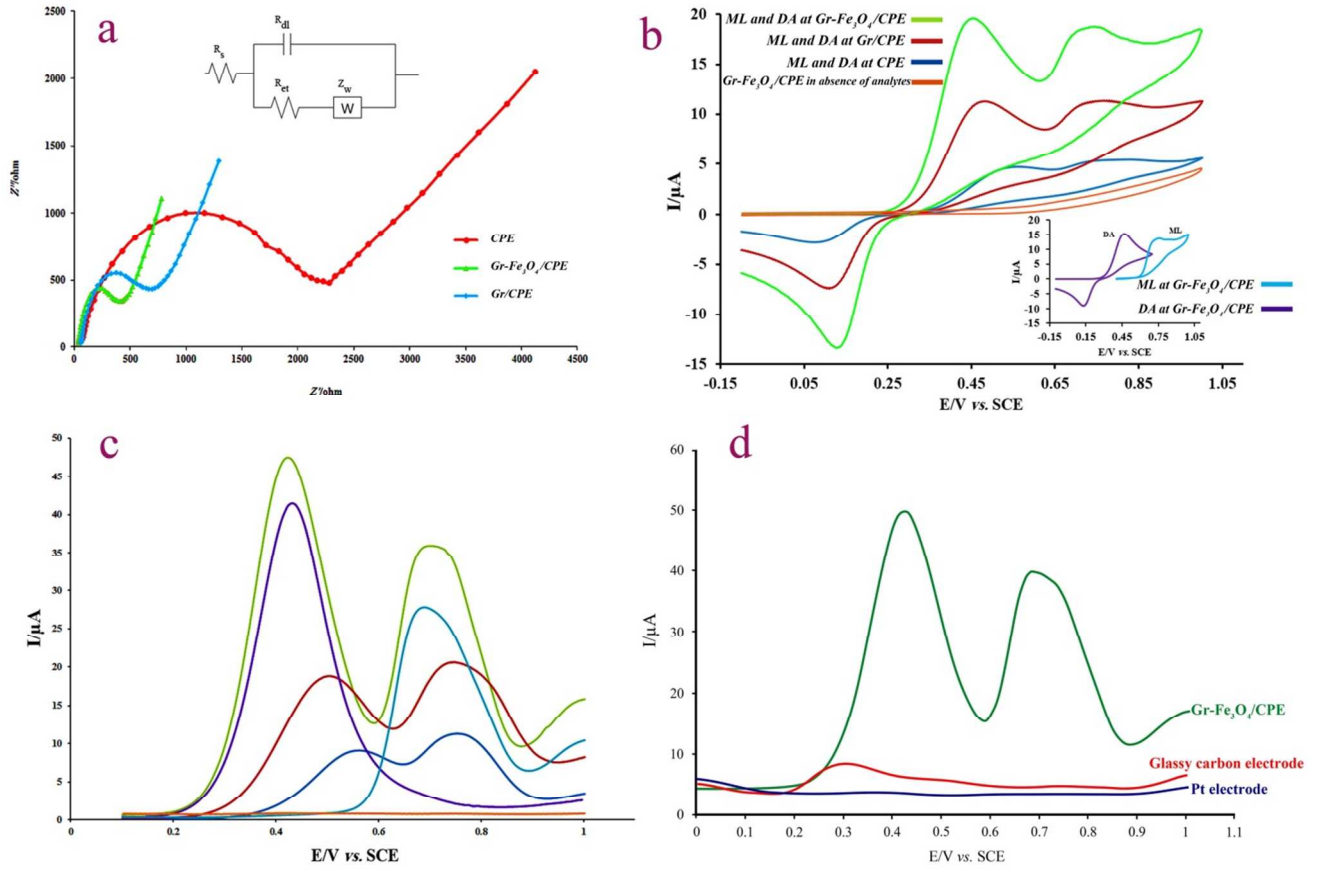

Fig. 2 EIS of different electrodes in 5.0 mM $Fe(CN)_6^{3-/4-}$ in B-R buffer solution (pH 5.0) (a), inset shows the equivalent circuit compatible with the Nyquist diagram for this system. (B) CVs for 4.0 μM ML and 4.0 μM DA (inset), and mixture of 4.0 μM ML and DA in B-R buffer solution (pH 5.0) on the surface of various electrodes and SWVs using prepared electrodes in different solutions (c). SWVs for mixture of 4.0 μM ML and DA in B-R buffer solution (pH 5.0) on the surface of Pt and glassy carbon in comparison with Gr-Fe_3O_4/CPE (d).

EIS has been used to monitor the electrochemical impedance changes at the different electrodes. Fig. 2a shows the EIS of bare CPE, Gr/CPE and Gr-Fe_3O_4/CPE in B-R solution containing 5.0 mM $Fe(CN)_6^{3-/4-}$. Fig. 2a inset shows the Randles equivalent circuit model, where the equivalence transfer resistance, solution transfer resistance, double layer capacitance and Warburg impedance, respectively. The total electrode impedance consists of the R_s in series with the parallel connection of the C_{dl} and Z_w. It is known that a large semi-circle for the electrode suggests high interfacial charge-transfer resistance, probably resulting from the poor electrical conductivity of active materials, while the inclined portion at lower frequencies is ascribed to the Warburg impedance, which is a consequence of the frequency dependence of ion diffusion/transport in the electrolyte to the electrode surface.[24,25] The Gr/CPE exhibited a depressed semicircle with an R_{ct} value of 78 Ω when compared with bare CPE (395 Ω), revealing the facilated electron transfer at Gr modified electrode. Also, Gr-Fe_3O_4/CPE showed a depressed semicircle with R_{ct} value of 42 Ω, validating its high conductivity and fast electron conducting ability at the electrode surface.[38]

Cyclic voltammograms of ML and DA

Fig. 2b shows the cyclic voltammograms (CVs) for 4.0 μM ML and DA at CPE, Gr/CPE and Gr-Fe_3O_4/CPE in B-R solution with pH=5.0. There were poor oxidation peaks and very close to each other in the CV responses of CPE. This indicates the slow electron transfer rates for the oxidation of these biomolecules at CPE. Such sluggish electron transfer kinetics may be related to the electrode fouling caused by the deposition of DA, ML, and their oxidation products on the electrode surface.[11] Electrode fouling is one of the biggest issues with electrochemical measurements of catecholamines and indoleamines. Following the oxidation of catecholamines and indoleamines, oxidative by-products are prone to adsorb on the electrode surface reducing the ability to conduct long-term measurements.[9,39] A single oxidation peak was observed for ML on the CPE electrode, suggestive of an irreversible redox reaction. The anodic peak potential was around 761 mV. For DA, the cathodic and anodic peaks appeared at CPE at 101 mV and 551 mV, respectively, and the peak potential separation is about 450 mV. Moreover, the anodic to cathodic peak current ratio is not equal to unity and cathodic peak current is very small compared to anodic peak current (Fig. 2b).

An obvious increase in the redox peak currents of ML and DA and a suitable peak potential difference were observed in

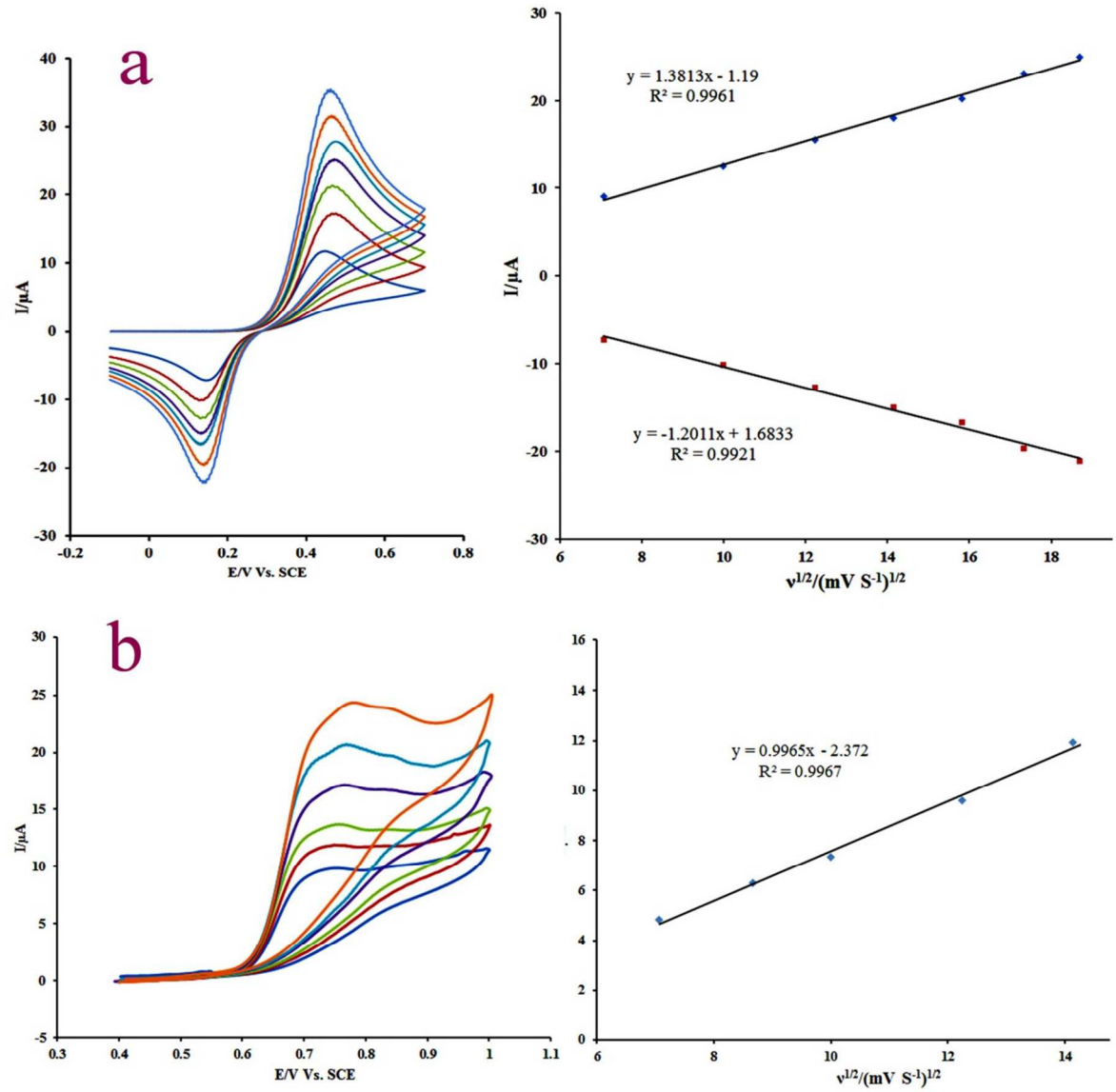

Fig. 3 CVs for Gr-Fe_3O_4/CPE in B-R buffer (pH 5.0) containing 4.0 μM of (a) DA with scan rates ranging from a to h as 50, 100, 150, 200, 250, 300 and 350 mV s^{-1},respectively, and (b) ML with scan rates ranging from a to f as 50, 75, 100, 200 and 250 mV s^{-1}. Insets show the linear relationship of the anodic peak current *vs.* square root of the scan rate ($\upsilon^{1/2}$).

the CV response of Gr/CPE, indicating the increase of electron transfer rate. Moreover, the enhanced peak current intensity was due to the special structure of Gr and the large surface area of Gr/CPE. The above results indicate that Gr/CPE had better electrochemical activity. For DA, the appearance of a well-defined redox couple with a 351 mV peak separation shows its reversibility on the Gr/CPE is much better than on bare CPE. This couple of redox peaks corresponds to two-electron oxidation of DA to dopaminequinone and the subsequent reduction of dopaminequinone to DA.[40,41] The improved reversibility could be due to the π-π interactions between the benzene ring of DA molecule and Gr layer, and the hydrogen bonds formed between hydroxyl or amine group in DA molecules and Gr layers. Onto Gr/CPE, the peak potential due to the oxidation of ML occurs at 713 mV (*vs* SCE) which is about 50 mV more negative than CPE. The observations on Gr/CPE demonstrate that a negative shift with much enhanced anodic peak current in comparison with CPE due to strong enhancement in the electron transfer rates of DA and ML is taking place. Also, the apparent peak shapes for DA and ML at Gr/CPE are improved against those at CPE, so that the well-shaped peaks of these species can be observed with the presence of Gr providing an excellent electrochemical reactivity. Moreover, no fouling was observed due to oxidation of DA or ML.

Fig. 2b demonstrates that Gr-Fe_3O_4/CPE can effectively increase the electro-oxidation of ML and DA and greatly improve the peak shapes. This can mainly be attributed to its large surface area and low surface resistance. The Gr-Fe_3O_4/CPE not only improves the redox peak currents but also

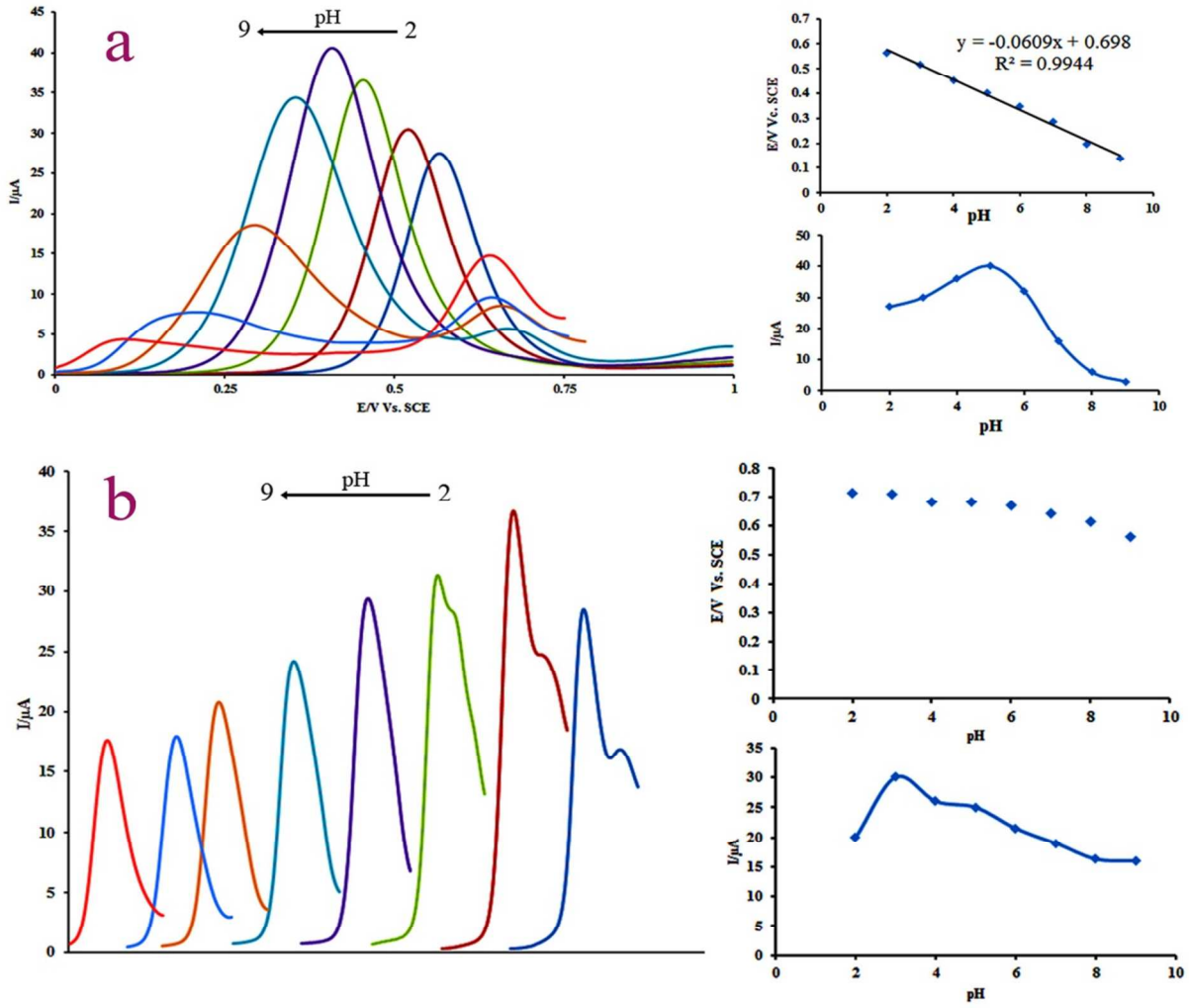

Fig. 4 (a) SWVs for Gr-Fe_3O_4/CPE in 4.0 μM DA at various pHs (pH 2.0–9.0) and effect of pH on the peak potentials and peak currents. (b) SWVs for Gr-Fe_3O_4/CPE in 4.0 μM ML at various pHs (pH 2.0–9.0), (B) effects of pH on the peak potentials and peak currents.

Fe_3O_4/CPE not only improves the redox peak currents but also makes the redox reaction of DA more reversible. This figure strongly suggests that the decorated Gr with Fe_3O_4 on the CPE can combine the advantages of all of them and increase surface area and electron transfer significantly; therefore, resulting in a remarkably increased response toward the redox reactions of ML and DA in contrast to the behavior from other electrode modifications.

SWV was applied for the electrochemical determination of ML and DA. As shown in Fig. 2c, the oxidation peaks of ML and DA at the Gr-Fe_3O_4/CPE had been improved obviously. For ML and DA, the oxidation peak potentials negatively shift comparing with their potentials at bare CPE. Moreover, the oxidation peak currents of ML and DA are 25 and 39 μA, which are about 4 and 5 times higher than their corresponded values at bare CPE, respectively. The significant increase of the oxidation peak current suggested that Gr-Fe_3O_4 have acted as promoter to facilitate the electrochemical oxidation of ML and DA. This can be ascribed to the intrinsic properties of Gr and Fe_3O_4 nanoparticles which lead to the significant increase in the oxidation peak current of target species. Two well-separated peaks corresponding to DA and ML appeared at 400 mV and 680 mV, respectively. The peak separation is about 280 mV on Gr-Fe_3O_4/CPE; sufficient for their simultaneous determination in samples containing these two compounds. Also, In order to compare the performance of fabricated electrode with Pt and glassy carbon electrodes, the SWVs of ML and DA using various electrodes were shown as Fig. 2d. As seen, no peak is observed on Pt electrode. A relatively broad and weak anodic peak with a peak potential of 0.3 V for the electro-oxidation of DA on the glassy carbon electrode reveals that the electrode process is very sluggish. On the basis of these observations, it can be postulated that Gr-Fe_3O_4/CPE exhibits effective electrochemical properties in the electrochemical oxidation of DA and ML in comparison with other electrodes.

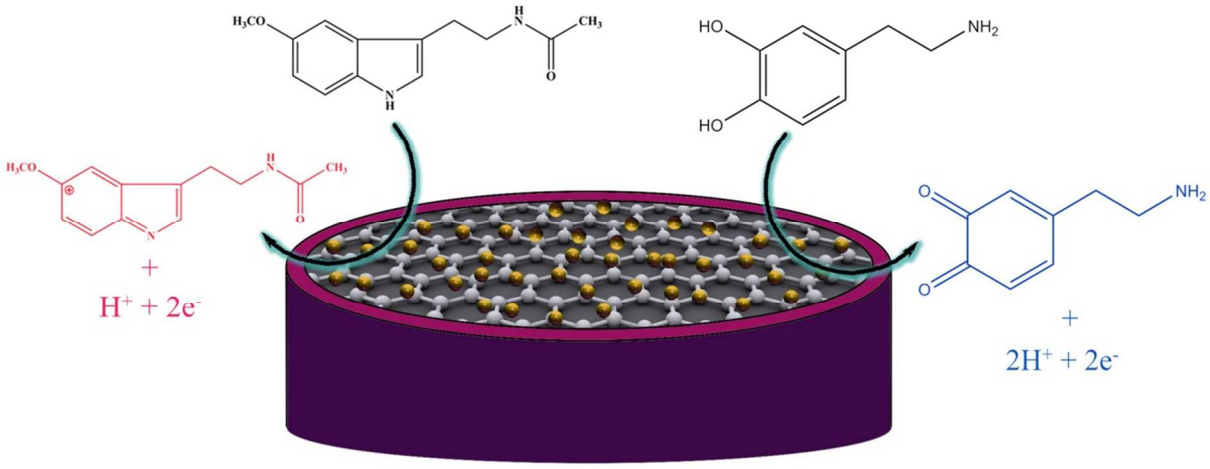

Scheme 1 Suggested pathways for possible oxidation of analytes (left) ML and DA (right).

Effect of scan rate

As we know, investigating the effect of scan rate on the oxidation peak current and peak potential can evaluate the kinetics of electrode reaction. The effect of scan rate on the electrochemical response of DA and ML was examined at various scan rates (Fig. 3). The results showed that the anodic peak currents vary linearly with the square root of scan rate ($\upsilon^{1/2}$) for both species, which confirm the diffusion controlled process for electrooxidation of DA and ML in the range 50.0-350.0 and 50.0-250.0 mV s^{-1}, respectively. For DA reduction, a linear relationship was also obtained for I *vs* log $\upsilon^{1/2}$ indicating a diffusion controlled process. Thus, rate-limiting adsorption and/or specific interactions at the Gr-Fe_3O_4/CPE surface are negligible. The regression equations were as follows:

I (μA) = 1.3813 $\upsilon^{1/2}$ -1.19 (R^2=0.9961) (For DA (oxidation))
I (μA) = -1.2011 $\upsilon^{1/2}$ -1.68 (R^2=0.9921) (For DA (reduction))
I (μA) = 0.9965 $\upsilon^{1/2}$ -2.37 (R^2=0.9967) (For ML)

Effect of pH

The choice of the supporting electrolyte is an important stage in electroanalytical studies because its composition and pH affect the properties of the solution as well as the electrode-solution interface, modifying the thermodynamics and kinetics of the charge transfer process, and the adsorption at the electrode surface. [42,43] Effects of various supporting electrolytes (B-R buffer, phosphate buffer, acetate buffer and KNO_3 solution) and pH were studied on the oxidation of ML and DA using Gr-Fe_3O_4/CPE. The anodic peak potentials for analytes are well separated in the four media, but the maximal peak currents of ML and DA were obtained in B-R buffer solution. Fig. 4 depicts the SW voltammograms of ML and DA in B-R buffer solution with different pHs. Anodic oxidation of ML follows a rather complex mechanism that is pH dependent. From pH 2.0 to 4.0, two close peaks were observed. These peaks might be related to the oxidation of the amine groups of ML. At pH 5.0, a single and well defined anodic wave was observed, meaning that the two peaks are completely superimposed in this pH. For DA, oxidation peaks with nice shape and high currents were recorded under acidic conditions (pH<6.0) in comparison with the peaks in B-R buffer solutions with pH values >6.0. As can be seen in Figs. 4a and b, the most well defined oxidation peak and the highest anodic current density was obtained in B-R buffer at pH 5.0. When the pH was more than 5.0, the peak current of DA was low, and voltammograms were appeared with two anodic peaks. Considering both the separation effect and the detection sensitivity, the buffer solution pH of 5.0 was chosen for the following measurements.

Though the elucidating the mechanism of ML and DA electrochemical oxidation is beyond the aim of this study, a short comment can be made. It is clear that the oxidation peak potentials of the two molecules shift to negative values with the increase of pH values. Linear relationships of the peak potential of DA as function of solution pH with slope 60.9 mV/pH, respectively are obtained (Fig. 4a). For DA, the slope is closed to the theoretical value of 59 mV/pH at 25◦C expected from the Nernst equation, indicates that the overall process of each molecule is proton dependent and the electron transfer is accompanied by the transfer of an equal number of protons. Two electrons and two protons are involved for the oxidation of DA to dopaminequinone and the subsequent reduction of dopaminequinone to DA. [4,5,10,11,17]

The obtained results on Gr-Fe_3O_4/CPE was almost similar to that shown in previous electrochemical investigations and it is suggested that the number of electrons transferred in the oxidation of ML is double that of protons. [12,42,44,45] It corresponds to the formation of cation at position 5 of indole ring. [42]

The reaction pathways for this step can be written as in Scheme 1.

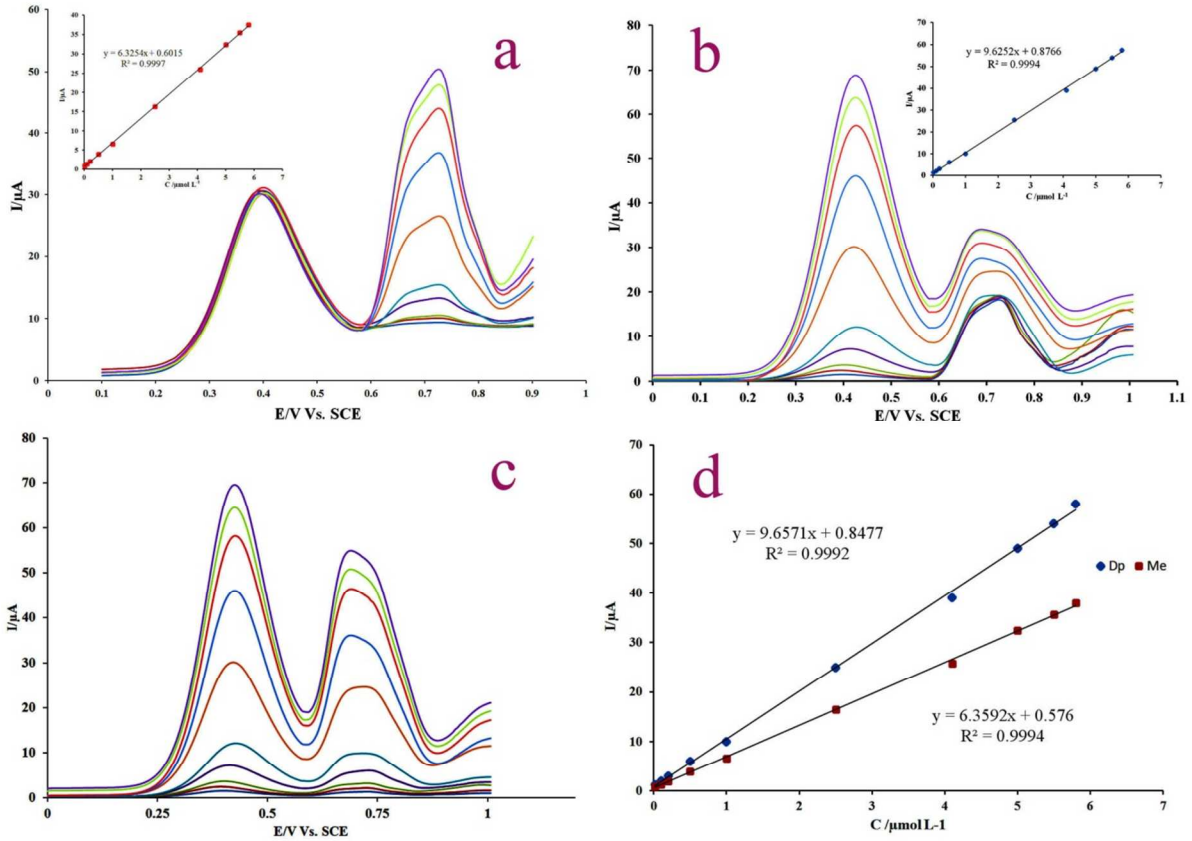

Fig. 5 (a) SWVs for ML at the Gr-Fe_3O_4/CPE in the presence of 2.5 μM DA in B-R buffer solution (pH = 5.0). (b) SWVs for DA at the Gr-Fe_3O_4/CPE in the presence of 2.5 μM ML (c) SWVs for different concentrations of DA and ML in pH 5.0 B-R buffer solution and calibration curves of ML and DA (d).

Simultaneous determination of ML and DA at Gr-Fe_3O_4 electrode

Fig. 5a displays the SWV obtained for the different concentrations of ML in the presence of 2.50 μM DA at Gr-Fe_3O_4/CPE. The oxidation peak current of ML has built up linearly (r=0.9998) with increasing concentration in the range of 0.02 to 5.80 μM, whereas the voltammetric peak current of DA remained the same. Similarly, voltammetric determination of DA was carried out in the presence of ML at fixed concentration being 2.50 μM. As shown in Fig. 5b, no obvious change in the oxidation current of ML was observed while varying concentration of DA and the peak current of DA increased linearly with increasing of its concentration 0.02 to 5.80 μM with a coefficient of determination of 0.9941. It should be concluded that the change of concentration of one studied species did not have the significant influence on the peak current and peak potential of the other one. Finally, it is very important to note that the oxidation processes of ML and DA on Gr-Fe_3O_4/CPE are independent.

Fig. 5c shows the SWVs obtained at Gr-Fe_3O_4/CPE for different concentrations of ML and DA in buffer solution with pH=5.0. The corresponding anodic currents of ML and DA increased linearly with increasing their concentrations over the range of 0.02 to 5.80 μM with the correlation coefficient of 0.9997 and 0.9996, respectively (Fig. 5d).

It was also found that observed oxidation peaks of ML and DA not only do not overlap with each other using Gr-Fe_3O_4/CPE electrode but also the peak current values are about equal to those obtained when the concentration of only one analyte changed in Figs. 5a, 5b and 5c. Thus, it can be concluded that Gr-Fe_3O_4/CPE is a sensitive electrochemical sensor for simultaneous determination of ML and DA. Further, our effort was focused on application of proposed method for analysis of biological fluid samples. The slope of the linear regression line for the calibration graph of each species is nearly equal to that without the other species, indicating that these two species do not interfere in the determination of each other.

Detection limits were estimated to be 8.4×10^{-3} μM for ML and 6.5×10^{-3} μM for DA based on $3s_b/m$, where s_b is the standard deviation of the mean value for 5 independent voltammetric response of the blank solution.

Interference studies

Under the same experimental conditions, potential interferences such as some ions and organic compounds were investigated by addition of possible interfereing species to mixture solution containing 1.0 μM ML and DA. It was observed that the common ions such as K^+, Na^+, Fe^{3+}, Cu^{2+}, Pb^{2+}, Al^{3+}, SO_4^{2-}, CO_3^{2-} and NO_3^- did not interfere with ML and

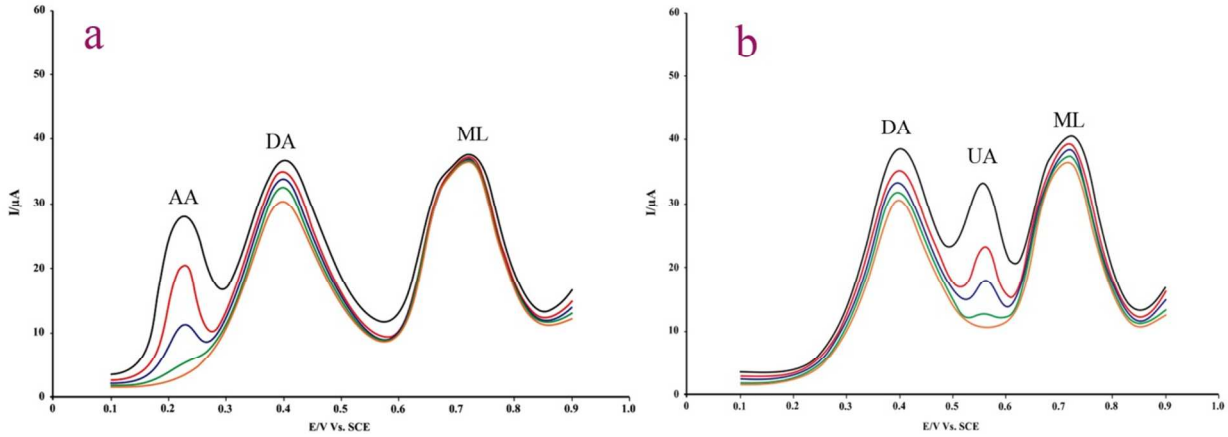

Fig. 6 (a) SWASV of DA and ML on Gr-Fe3O4/CPE (a) in the presence of AA (5.0-15.0 μM) and (b) in the presence of UA (1.0-18.0 μM).

Table 1 Results for ML and DA determination (μM) in real samples obtained under the optimum conditions (N=7).

Samples	Analyte	Added (μM)	Found	Recovery (%)	Official Method
Urine	ML	0.00	0.00	-	-
		2.50	2.49	99.6	2.47
		3.50	3.55	101.4	3.52
	DA	0.00	0.00	-	-
		3.00	2.96	98.6	2.90
		5.00	4.97	99.4	5.20
Serum	ML	0.00	0.00	-	-
		2.50	3.12	104.0	2.47
		3.50	3.46	98.8	3.51
	DA	0.00	0.00	-	-
		3.00	2.91	97.0	2.99
		5.00	5.16	103.2	5.13
DA Injection	DA	0.00	0.51	-	0.49
		1.00	1.49	96.0	1.50
		2.00	2.50	98.0	2.48
	ML	0.00	0.00	-	-
		0.50	0.49	98.0	0.52
		1.00	0.97	97.0	0.99
ML Tablet	DA	0.00	0.00	-	-
		1.00	1.04	104.0	1.02
		2.00	1.98	99.0	1.97
	ML	0.00	0.80	-	0.79
		0.50	1.28	97.5	1.30
		1.00	1.82	102.5	1.83

Table 2 Comparison of some figures of merit related to the different modified electrodes for the (individual or simultaneous) determination with priority of ML accompanying DA.

Electrode	Method	Linear range (μM)		Detection limit (μM)		Simultaneously with other analytes	Refs.
		ML	DA	ML	DA		
CPE	CV	6.0×10^{-2}- 8.0×10^{-1}	-	3.0×10^{-2}	-	Alone	6
Activated GCE	LSV	8.0×10^{-1} -10.0[1]	-	5.0×10^{-2}	-	Alone	7
Boron-doped diamond electrode	DPV	344.4-688.8	-	10.3		Alone	9
MWCNTs/DHP/GCE [a]	LSV	8.0×10^{-2} – 10.0	-	2.0×10^{-2}	-	Alone	12
Boron-doped diamond electrode	DPV	5.0×10^{-1} – 4.0	-	1.1×10^{-1}	-	Alone	42
MWCNTs-CHNPs/ CILE [b]	DPV	LSV	-	4.0×10^{-3}	-	levodopa	44
CPE	CV	3.0-550.0	-	2.30	-	Alone	45
HMDE	SWCASV	1.0×10^{-3} -1×10^{-1}	-	3.1×10^{-4}	-	Alone	48
Castor oil-CPE	DPV	5.0×10^{-2} -1.0×10^{-1}	-	1.0×10^{-9}	-	Alone	49
Manganese Hexacyanoferrate with Poly(3,4-ethylene dioxythiophene) Hybrid Film Modified GCE	CV Amperometry	100.0-460.0	-	10.0	-	Catechin	50
CPE	CV ACV	1.0×10^{-2} -4.0×10^{-1} 1.0×10^{-4} -1×10^{-3}	-	5.0×10^{-2} 9.0×10^{-5}	-	Alone	51
CNT/GO/CS/GCE CNT/GO/sCS/GCE [c]	Amperometry	-	0.06 0.06	1.25-280 1.25-357	-	uric acid and ascorbic acid	52
MIPs@CuO@GCE	CV		2.0×10^{-2}– 25		8×10^{-3}	Alone	53
Molecularly bioimprinted polymer	DPV		0.02 – 7		6×10^{-3}	Alone	54
ZnO nanorods modified CPE	SWV	N.R.	0.3- 10.0 and 10.0 to 100.0	N.R.	56×10^{-3}	methionine and caffeine	55
Gr-Fe_3O_4/CPE	SWV	2.0×10^{-2} – 5.8	2.0×10^{-2} – 5.8	8.4×10^{-3}	6.5×10^{-3}	-	This work

a) Multi-walled carbon nanotubes/dihexadecyl hydrogen phosphate; b) Multi-walled carbon nanotubes/cobalt hydroxide nanoparticles and (c) Carbon nanotubes/graphene oxide/ sulfonated chitosan-modified glassy carbon electrode.

DA. No interfering peaks were also recorded around the peak potentials of ML and DA in 60-fold excess of common urinary compounds such as glucose, urea, uric acid (UA) and AA (signal change ±5%). As an illustrated example, UA oxidized at +0.572 V *vs.* SCE, thus some difficulties about overlapping the oxidation peaks of UA and ML could occur in very high concentration of UA. But as it is evident from Fig. 6, good potential separation was observed in 60-fold excess of UA. These facts prove the good selectivity of the proposed method and offer the promising possibilities for simultaneous determination of DA and ML in presence of UA.

There has a great importance to determine ML simultaneously in the presence of other biological indoles. ML oxidation occurred at a potential of 0.70 mV. This potential is well distinguished from those of the melatonin precursor, serotonin (Ep = 300 mV) and dihydroxytryptamine (0.180 mV). This suggests that melatonin could be selectively analyzed in the presence of serotonin and dihydroxytryptamine. indole or tryptamine and other oxidizable compounds that are found naturally in body fluids, *e.g.*, AA and UA. The interferences caused by a 12-fold excess of tryptophan was serious. Because tryptophan has similar electroactive group as ML, thus affect the oxidation peak current of ML.

Determination of ML and DA in real samples

The proposed method was applied to simultaneously determination of ML and DA in pharmaceutical samples and biological fluids in order to demonstrate the capability of the fabricated sensor. Results obtained by this method were compared with those obtained by official methods.[45,46] It was concluded no significant difference between the two methods.

The feasibility of prepared sensor for the real samples analysis was further examined by the recovery test. The results (Table 1) showed that suggested method using the Gr-Fe_3O_4/CPE produced satisfactory recovery results.

Conclusions

In the present study, for the first time, sensitive, inexpensive, rapid and selective method for simultaneous determination of two important species present in the biological fluids and pharmaceutical samples (ML and DA) was proposed based on their oxidation on the Gr-Fe_3O_4/CPE using SWV technique. Compared with other electrodes (shown in Table 2), the proposed electrode shows excellent advantages such as wide linear ranges and low LODs. Ease of preparation, high sensitivity and stability, low detection limit, fast response, as well as satisfied peak separation in the system reported here, can make it possible to successfully determine sub micromolar concentration of these analytes individually or simultaneously in different samples without any separation or pretreatment step.

Acknowledgments

This research was supported by the Research Office of the Baqiyatallah University of Medical Sciences. We thank Dr. Alireza Shahriyari for his valuable comments.

Notes

[a] *Chemical Injuries Research Center, Baqiyatallah University of Medical Sciences, Tehran, Iran.*
[b] *Faculty of Chemistry, Bu-Ali Sina University, Hamedan, Iran.*

References

1 D. Bonnefont-Rousselot and F. Collin, *Toxicology*, 2010, **278**, 55-67.
2 T. Meng, Z.H. Zheng, T.T. Liu and L. Lin, *Neurochem. Res.,* 2012, **37**, 1050-1056.
3 S. Yano, K. Moseley and C. Azen, *J. Pediatr.*, 2013, **162**, 999-1003.
4 D.P. Quan, D.P Tuyen, T.D. Lam, P.T. N. Tram, N. H. Binh and P.H. Viet, *Colloids Surf. B*, 2011, **88**, 764-770.
5 D.M. Fernandes, M. Costa, C. Pereira, B. Bachiller-Baeza, I. Rodriguez-Ramos, A. Guerrero-Ruiz and C. Freire, *J. Colloid Interf. Sci.*, 2014, **432**, 207-213.
6 J.L. Corujo-Antuna, E.M. Abad-Villar, M.T. Fernandez-Abedul and A. Costa-Garcia, *J. Pharm. Biomed. Analysis*, 2003, **31**, 421-429.
7 W. Xiao-Ping, Z. Lan, L. Wen-Rong, D. Jian-Ping, C. Hong-Qing and C. Guo-Nan, *Electroanalysis*, 2002, **14**, 1654-1660.
8 M.S. Talebianpoor, S. Khodadoust, A. Rozbehi, M. Akbartabar Toori, M. Zoladl, M. Ghaedi, R. Mohammadi and A.S. Hosseinzadeh, *J. Chromatogr. B*, 2014, **960**, 1-7.
9 A.T. Ball and B.A. Patel, *Electrochim. Acta*, 2012, **83,** 196-201.
10 K. Jackowska and P. Krysinski, *Anal. Bioanal. Chem.*, 2013, **405**, 3753-3771.
11 A. Safavi, N. Maleki, O. Moradlou and F. Tajabadi, *Anal. Biochem.,* 2006, **359**, 224-229.
12 W.Y. Qu, F. Wang, S.S. Hu and D.F. Cui, *Microchim Acta*, 2005, **150**, 109-114.
13 H. Bagheri, A. Afkhami, Y. Panahi, H. Khoshsafar and A. Shirzadmehr, *Mater. Sci. Eng. C*, 2014, **37**, 264-270.
14 A. Afkhami, H. Bagheri, H. Khoshsafar, M. Saber-Tehrani, M. Tabatabaee and A. Shirzadmehr, *Anal. Chim. Acta*, 2012, **746**, 98-106.
15 H. Bagheri, A. Afkhami, H. Khoshsafar, M. Rezaei and A. Shirzadmehr, *Sens. Actuators B*, 2013, **186**, 451-460.
16 N. Rodthongkum, N. Ruecha, R. Rangkupan, R.W. Vachet and O. Chailapakul, *Anal. Chim. Acta,* 2013, **804**, 84-91.
17 X.H. Zhu, Y. Liang, X.O. Zuo, R.P. Hu, X. Xiao and J.M. Nan, *Electrochim. Acta*, 2014, **143**, 366-373.
18 A. Afkhami, A. Shirzadmehr, T. Madrakian and H. Bagheri, *Talanta*, 2015, **131**, 548-555.
19 A. Martin and A. Escarp, *Trends Anal. Chem.,* 2014, **56**, 13-26.
20 S. Stankovich, D.A. Dikin, G.H.B. Dommett, K.M. Kohlhaas, E.J. Zimney, E.A. Stach, R.D. Piner, S.T. Nguyen and R.S. Ruoff, *Nature*, 2006, **442**, 282-286.
21. Z. Wang, X. Zhang, Y. Li, Z.T. Liu and Z.P. Hao, *J. Mater. Chem. A*, 2013, **1**, 6393-6399.
22 T.Q. Xu, Q.L. Zhang, J.N. Zheng, Z.Y. Lv, J. Wei, A.J. Wang and J.J. Feng, *Electrochim. Acta*, 2014, **115**, 109-115.
23 B. Kaur, T. Pandiyan, B. Satpati and R. Srivastava, *Colloids Surf. B*, 2013, **111**, 97-106.
24 A. Afkhami, H. Khoshsafar, H. Bagheri and T. Madrakian, *Sens. Actuators B*, 2014, **203**, 909-918.
25 A. Afkhami, H. Khoshsafar, H. Bagheri and T. Madrakian, *Anal. Chim. Acta*, 2014, **831**, 50-59.
26 Y.H. Song, Z.F. He, H.Q. Hou, X.L. Wang and L. Wang, *Electrochim. Acta*, 2012, **71**, 58-65.
27 H. Teymourian, A. Salimi and S. Khezrian, *Biosens. Bioelectron.*, 2013, **49**, 1-8.
28 H. Bagheri, A. Afkhami, M. Saber-Tehrani and H. Khoshsafar, *Talanta*, 2012, **97**, 87-95.
29 Y.Q. Wang, H.J. Zhang, D. Yao, J.J. Pu, Y. Zhang, X.R. Gao and Y.M. Sun, *J. Solid State Electrochem.*, 2013, **17**, 881-887.
30 T.A.P. Rocha-Santos, *Trends Anal. Chem.*, 2014, **62**, 28-36.
31 Y.Q. Wang, Q. Liu, Q. Qi, J.J. Ding, X.R. Gao, Y. Zhang and Y.E. Sun, *Electrochim. Acta*, 2013, **111**, 31-40 .
32 W.S. Hummers and R.E. Offeman, *J. Am. Chem. Soc.*, 1958, **80**, 1339-1339.
33 J. Su, M.H. Cao, L. Ren and C.W. Hu, *J. Phys. Chem. C*, 2011, **115**, 14469-14477.
34 J. Qian, L. Jiang, X.W. Yang, Y.T. Yan, H.P. Mao and K. Wang, *Analyst*, 2014, **139**, 5587-5593.
35 Y.F. Sun, W.K. Chen, W.J. Li, T.J. Jiang, J.H. Liu and Z.G. Liu, *J. Electroanal. Chem.*, 2014, **714-715**, 97-102.
36 H.L. Guo, X.F. Wang, Q.Y. Qian, F.B. Wang and X.H. Xia, *ACS Nano*, 2009, **3**, 2653-2659.
37 H.M. Sun, L.Y. Cao and L.H. Lu, *Nano Res.*, 2011, **4**, 550-562.
38 W. Shi, J. Zhu, D.H. Sim, Y.Y. Tay, Z. Lu, X. Zhang, Y. Sharma, M. Srinivasan, H. Zhang, H.H. Hng and Q. Yan, *J. Mater. Chem.*, 2011, **21**, 3422-3427.
39 A. Salimi, H. Mam-Khezri and R. Hallaj, *Talanta*, 2006, **70**, 823-832.
40 P. Kalimuthu and S.A. John, *Bioelectrochemistry*, 2009, **77**, 13-18.
41 A. Afkhami, D. Nematollahi, T. Madrakian and L. Khalafi, *Electrochim. Acta*, 2005, **50**, 5633-5640.

42 A. Levent, *Diam. Relat. Mater.*, 2012, **21**, 114-119.
43 H. Bagheri, H. Karimi-Maleh, F. Karimi, Sh. Mallakpour and M. Keyvanfard, *J. Mol. Liq.*, 2014, **198**, 193-199.
44 A. Babaei, A.R. Taheri and I. Khani Farahani, *Sens. Actuators B*, 2013, **183**, 265-272.
45 A. Radi and G.E. Bekhiet, *Bioelectroch. Bioener.*, 1998, **45**, 275-279.
46 V. Rizzo, C. Porta, M. Moroni, E. Scoglio, R. Moratti, *J Chromatogr. B*, 2002, **774**, 17-24.
47 L. Eb and W. Hq, *A Service of the U.S. National Library of Medicine and the National Institutes of Health*, 2005, **25**, 1213.
48 A.M. Beltagi, P.Y. Khashaba and M.M. Ghoneim, *Electroanalysis*, 2003, **15**, 1121-1128.
49 A. Radi, *Anal. Commun.*, 1999, **36**, 43-44.
50 T.H. Tsai, Y.C. Huang and S.M. Chen, *Int. J. Electrochem. Sci.*, 2011, **6**, 3238-3253.
51 J.L. Corujo-Antuna, S. Martinez-Montequin, M.T. Fernandez-Abedul and A. Costa-Garcia, *Electroanalysis*, 2003, **15**, 773-778.
52 Y. T. Shieh and H. F. Jiang, *J. Electroanal. Chem.* 2015, **736**, 132-138.
53 Li, B., Zhou, Y., Wu, W., Liu, M., Mei, S., Zhou, Y., and Jing, T, *Biosens. Bioelectron.*, 2014, **67**, 121-128.
54 B. Rezaei, M. K. Boroujeni, and A. A. Ensafi, *Biosens. Bioelectron.*, 2015, **66**, 490-496.
55 E. Molaakbari, A. Mostafavi, and H. Beitollahi *Sens. Actuators, B*, 2015, **208**, 195-203.

